Journal of the Optical Society of America B
OPTICAL PHYSICS

Design of simultaneous multicolor coherent light generation in a single MgO:PPLN bulk crystal

Dismas K. Choge,[1,*] David W. Waswa,[1] Kennedy M. Muguro,[1] and Wan-Guo Liang[2]

[1]University of Eldoret, Eldoret 30100, Kenya
[2]Fujian Institute of Research on the Structure of Matter, Chinese Academy of Sciences, Fuzhou 350002, China
*Corresponding author: dchoge@uoeld.ac.ke

Received 2 June 2020; revised 28 July 2020; accepted 5 August 2020; posted 6 August 2020 (Doc. ID 399164); published 14 September 2020

We report on simultaneous sum-frequency mixing and doubling of C-band and ~980 nm laser sources using a single segmented periodically poled lithium niobate (PPLN) crystal in a single-pass configuration. Our theoretical analysis on the spectral outputs show that a proper design of a five-segment single PPLN crystal has potential to generate violet, blue, green, and orange wavelengths by simultaneous sum-frequency and second-harmonic generation processes. Such a design has promising potential for a compact, tunable multicolored laser that can find various applications such as in biomedicine, visible light communications, laser-based color displays, and sensing.

https://doi.org/10.1364/JOSAB.399164

1. INTRODUCTION

Laser sources in the visible region have become indispensable in our society motivated by diverse cutting-edge scientific and technological application areas, including biomedicine [1], laser projection displays [2], visible light communications [3], and sensing [4]. Nonlinear optical crystal such as lithium niobate (LN) offers viable design flexibility for quasi-phase-matching (QPM), which facilitates implementation of such laser sources by spatially modulating the sign of nonlinearity [5]. QPM second-harmonic generation (SHG), third-harmonic generation (THG), and sum-frequency generation (SFG) are among the attractive techniques for generating visible light. Additionally, QPM allow access to the highest nonlinear coefficient d_{33} and is free of walk-off, which makes it possible to utilize long interaction lengths crucial for attainment of practical powers. On the other hand, multiperiodic poling of LN offers an advantage of achieving simultaneous QPM processes within a single crystal or in a cascaded module. Previously, this technique has been used to create a coherent source of the three primary colors: red (R), green (G), and blue (B), for instance, by using a cascade of nonlinear crystals each for a different nonlinear process [6], self-frequency doubling, and self-frequency mixing in Nd^{3+}-doped bulk aperiodically poled lithium niobate [7,8]. Red, yellow, green, and blue light in a single aperiodically poled lithium tantalate (LT) [9,10] has also been demonstrated, as well as simultaneous RGB generation in periodically poled lithium niobate (PPLN) with ultrabroadband optical parametric generation (OPG) [11]. Cascaded nonlinear interactions in a single stoichiometric LT with two periodicities have been used to demonstrated RGB laser generation [12,13]. We have previously demonstrated a blue and orange dual-color source in a single period magnesium-oxide-doped PPLN (MgO:PPLN) crystal via simultaneous SFG and SHG processes [14].

Here we numerically evaluate simultaneous single-pass SFG and SHG wavelength conversion in a five-segment step-chirped PPLN (SC-PPLN) grating structure and show that visible light at multiple wavelengths with tunable properties can be achieved. The approach utilizes a different grating period in each segment designed to quasi-phase-match either SHG or SFG process. This design scheme has potential for a compact, robust, and tunable multicolored source of visible light within a single crystal.

2. PPLN DESIGN

The QPM grating structure shown in Fig. 1 is assumed to be implemented in a z-cut x-propagating MgO:PPLN bulk crystal and consists of five segments ($m = 5$) with total device length L. The periods are denoted as Λ_l where $l = 1, 2, \ldots m$.

For $m = 1$, 2, and 5 intended for SFG, the coupled mode equations are expressed as [15]

$$\frac{dA_{1,m}}{dz} = -\frac{2i\omega_{1,m}}{n_{1,m}c} d_{\text{eff}} A_{3,m} A^*_{2,m} \exp(-i\Delta k_m z), \quad (1)$$

$$\frac{dA_{2,m}}{dz} = -\frac{2i\omega_{2,m}}{n_{2,m}c} d_{\text{eff}} A_{3,m} A^*_{1,m} \exp(-i\Delta k_m z), \quad (2)$$

$$\frac{dA_{3,m}}{dz} = -\frac{2i\omega_{3,m}}{n_{3,m}c} d_{\text{eff}} A_{3,m} A_{2,m} \exp(i\Delta k_m z), \quad (3)$$

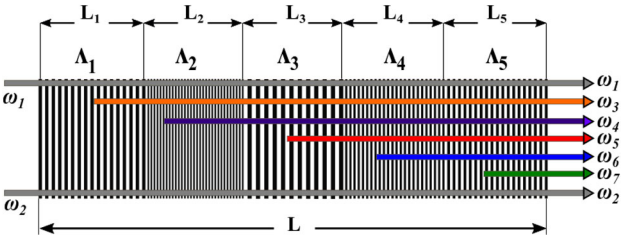

Fig. 1. Five-segment SC-PPLN grating structure.

where $A_{1,m}$, $A_{2,m}$, and $A_{3,m}$ denote the amplitudes of the ($\omega_{1,m}$), signal ($\omega_{2,m}$), and idler ($\omega_{3,m}$), respectively; c is the speed of light in a vacuum, and z is the distance along the direction of propagation. Here, the subscript m denotes either the first, second, or the fifth segment. The phase mismatch due to material dispersion is expressed as [16]

$$\Delta k_m = k_{1,m} + k_{2,m} - k_{3,m} - \frac{2\pi}{\Lambda_m}. \tag{4}$$

The temperature-dependent refractive indices $n_{1,m}$, $n_{2,m}$, and $n_{3,m}$ are calculated using the Sellmeier equations, and $d_{\text{eff}} = -\frac{2d_{33}}{\pi}$ ($d_{33} = 27$ pm/V) is the effective nonlinear coefficient of MgO:PPLN [17]. This highest nonlinearity can be accessed when all the three interacting waves are polarized along the optical axis of the MgO:PPLN crystal. For SHG in the third and fourth segments, the coupled mode equations take the form

$$\frac{dA_j}{dz} = -\frac{2i\omega_j}{n_j c} d_{\text{eff}} A_{j+4} A_j^* \exp(-i\Delta k_m z), \tag{5}$$

$$\frac{dA_{j+5}}{dz} = -\frac{2i\omega_{j+4}}{n_{j+4} c} d_{\text{eff}} A_j^2 \exp(i\Delta k_m z), \tag{6}$$

where $j = 1, 2$ for pump and signal, respectively, while the phase mismatch is

$$\Delta k = k_{j+1} + 2k_j - \frac{2\pi}{\Lambda_m}, \tag{7}$$

where A_{j+1} is the amplitude of the second harmonic of ω_1 at ω_5 and ω_2 at ω_6, and $m = 3, 4$. The normalized conversion efficiencies for SFG and SHG processes are estimated as the power ratio between the output SFG/SHG power and the product of the input power, which are expressed respectively as

$$\eta_{\text{SFG}} = \frac{P_{\text{SFG}}}{(P_1 P_2)} W^{-1}, \tag{8}$$

$$\eta_{\text{SHG}} = \frac{P_{\text{SHG}}}{(P_1 P_2)^2} W^{-1}. \tag{9}$$

For single-pass SFG and SHG configurations, Eqs. (1)–(3) and (5)–(6) are simultaneously solved assuming undepleted pump regime and negligible propagation losses.

Figure 2 shows a schematic of the multiwavelength conversion based on cascaded processes in the proposed SC-PPLN depicted in Fig. 1. A tunable pump ($P_1 = 2$ W) in the wavelength range from 1500 to 1600 nm (λ_1) is supposedly injected in to the PPLN along with a fixed signal ($P_2 = 1$ W) at central wavelength of 980 nm (λ_2). As the pump and the signal propagate through the first segment of PPLN crystal, it generates an idler light in the 600 nm wavelength (λ_3) range by sum-frequency interaction; $1/\lambda_3 = 1/\lambda_1 + 1/\lambda_2$. The sum-frequency idler then interacts (sum-frequency interaction) with the pump in the second segment of the crystal, leading to generation of a second idler in the 432 nm (λ_4) wavelength range; $1/\lambda_4 = 1/\lambda_1 + 1/\lambda_3$. By frequency doubling of the pump, 775 nm wavelength ($\lambda_5 = \lambda_1/2$) is generated in third segment followed by frequency doubling of the residual signal in the fourth segment to generate 490 nm wavelength ($\lambda_6 = \lambda_2/2$) output. In the last segment, sum-frequency mixing of the pump and its second harmonic yields a third idler (third harmonic generation) output at 515 nm wavelength ($\lambda_7 = \lambda_1/3$). The simultaneous processes are dependent on the temperature of the crystal, phase mismatch between the pump, signal, and the three idlers, while the conversion efficiency depends on the proper phase matching and the fundamental powers.

3. RESULTS AND DISCUSSION

We simulated the SFG and SHG processes by solving the coupled mode equations (using the ordinary differential equations

Table 1. Summary of the Device Design Parameters

Process	Λ_{QPM} (μm) at 25°C[a]	Segment Length (mm)	Expected Output Wavelength (nm)
SFG($\omega_1 + \omega_2 \rightarrow \omega_3$)	10.4	10	600
SFG($\omega_1 + \omega_3 \rightarrow \omega_4$)	4.3	10	432
SHG($\omega_1 \rightarrow \omega_5$)	19.4	10	775
SHG($\omega_2 \rightarrow \omega_6$)	5.4	10	490
SFG($\omega_1 + \omega_5 \rightarrow \omega_7$)	7.0	10	515

[a]Calculated with SNLO (AS photonics).

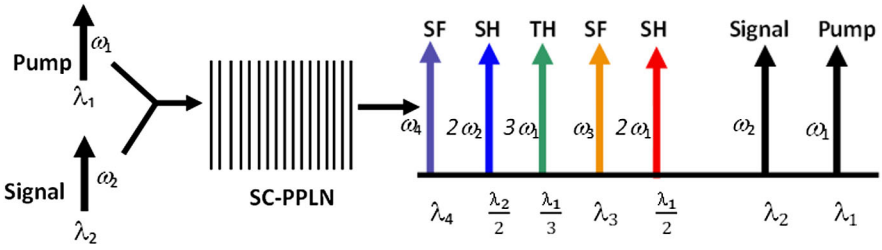

Fig. 2. Schematic of multiple wavelength conversion based on cascaded SHG-SFG processes in segmented PPLN. SF, sum frequency; SH, second harmonic; TH, third harmonic.

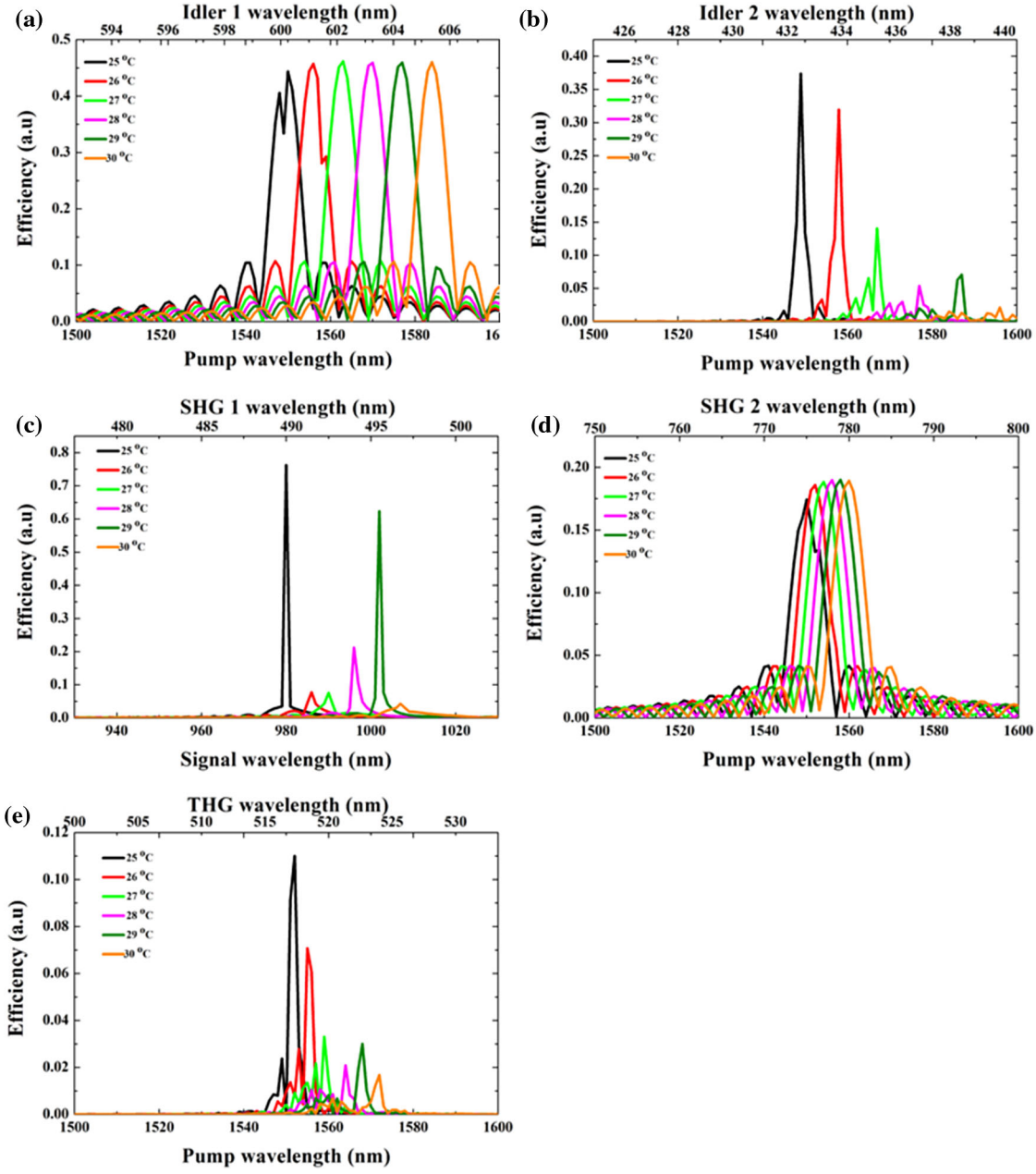

Fig. 3. Efficiency as a function of pump and signal wavelengths at various temperatures for (a) 600 nm (SFG 1), (b) 432 nm (SFG 2), (c) 490 nm (SHG 1), (d) 775 nm (SHG 2), and (e) 515 nm (THG) spectral regions.

solver in MATLAB) for each section using the QPM periods predicted with SNLO (AS photonics) [18] for MgO:PPLN (see Table 1). We assumed that both the pump and the signal are highly monochromatic and undepleted. The powers of the input light sources are assumed to be 2 W and 1 W for the pump and signal, respectively, and these together with the output of the previous section act as the inputs for the next section in the calculation. The wavelength of the tunable pump laser was increased in steps of 0.001 nm. For comparison, we assume that the five segments are of equal length (L = 10 mm). Figure 3 shows the simulated conversion efficiencies of both idler 1 and 2 generated by sum-frequency interaction (segments 1 and 2), second harmonic (segments 3 and 4), and third harmonic (segment 5) along with pump and signal wavelengths. The corresponding idler, second-harmonic wavelength, and third-harmonic wavelength are shown in the upper horizontal axes. Here, the PPLN temperature is increased in steps of 1°C from 25°C to 30°C. According to Fig. 3, as temperature increased, the generated idlers shifted to longer wavelengths within the visible range as expected. As can be seen in Figs. 3(a) and 3(d), the shape of the converted spectra does not change, a property that can be utilized to change the operation wavelength of the device. As shown in Fig. 3(c), it is possible to switch the output wavelength by tuning the temperature from 25°C and 27°C and still achieve comparable conversion efficiency. When the temperature is increased, the conversion efficiencies for idler 2

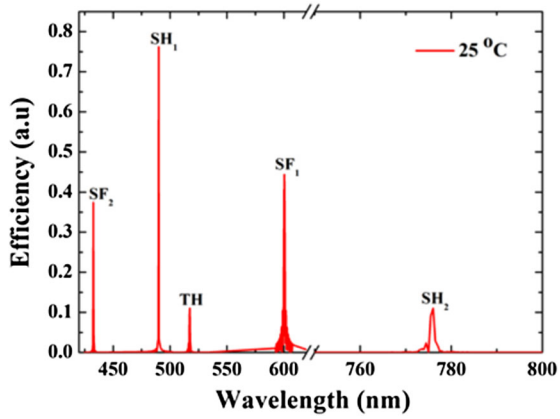

Fig. 4. Overlaying of five simulated spectra including SFG of two pumps at 1549 nm and 1550 nm, SHG of pump and signal at 1550 nm and 980 nm, respectively, and THG at 1550 nm named as SF for the sum-frequency mixing, SH for the second-harmonic generation, and TH for third-harmonic generation.

and THG will decrease according to Figs. 3(b) and 3(e). In spite of the slight fluctuation of the efficiency with temperature, it can be concluded that the proposed device can work properly near room temperature. Furthermore, the device can fulfill the tunability requirement by changing the temperature. For instance, it is possible to access up to 5.0 nm in the 600 nm spectral region (SFG 1) by simply changing the temperature as shown in Fig. 3(a). Similarly, up to 7.2 nm in the 432 nm region (SFG 2), 2.5 nm in the 490 nm region (SHG 1), 5.0 nm in the 775 nm region (SHG 2), and 6.7 nm in the 515 nm region (THG) as shown in Figs. 3(b)–3(e). For the results shown in Fig. 3(c), the signal is tuned from 965 to 1000 nm in steps of 0.001 nm.

Figure 4 shows the overlaying of simulated spectra for SFG 1 (idler 1), SFG 2 (idler 2), SHG 1, SHG 2, and THG for different pumps centered at 1550, 1549, and 1552 nm and the signal at 980 nm when the temperature is fixed at 25°C. It can be seen that the conversion efficiencies for SFG 1, SFG 2, SHG 1, SHG 2, and THG are approximately 44%, 37%, 76%, 11%, and 11% respectively.

Therefore, by tuning the pumps in the range of 1549 to 1552 nm for a fixed signal, all the desired nonlinear processes are satisfied simultaneously although with disparities in the conversion efficiencies. In practice, however, there exist imperfections in the domain pattern due to fabrication errors that could degrade the conversion efficiencies of the simultaneous processes. Figure 5 shows the calculated wave vectors for SFG 1, SFG 2, SHG 1, SHG 2, and THG. The results presented here are for central wavelengths of 1550, 980, and 600 nm for pump, signal, and idler 1, respectively. Here we used the numerical method proposed in Ref. [19], where the beam waist of 100 μm was assumed for the input lasers, although this is not the optimized value. At the end of each section, K_x and K_y wavevector components are seen to be wider compared to the fundamental beams in the spatial spectra, which is expected due to different wavelengths.

4. CONCLUSION

We have reported a theoretical and numerical analysis of single-pass simultaneous wavelength conversion in a five-segment QPM grating structure to generate CW visible light at multiple wavelengths. The analysis on the spectral outputs shows possible temperature tuning to access up to 5.0, 7.2, 2.5, 6.7, and 5.0 nm in the 600, 432, 490, 515, and 775 nm spectral regions, respectively. Such design scheme offers a promising potential for a compact, robust, and tunable multicolored source of visible light within the same crystal, which can find applications in

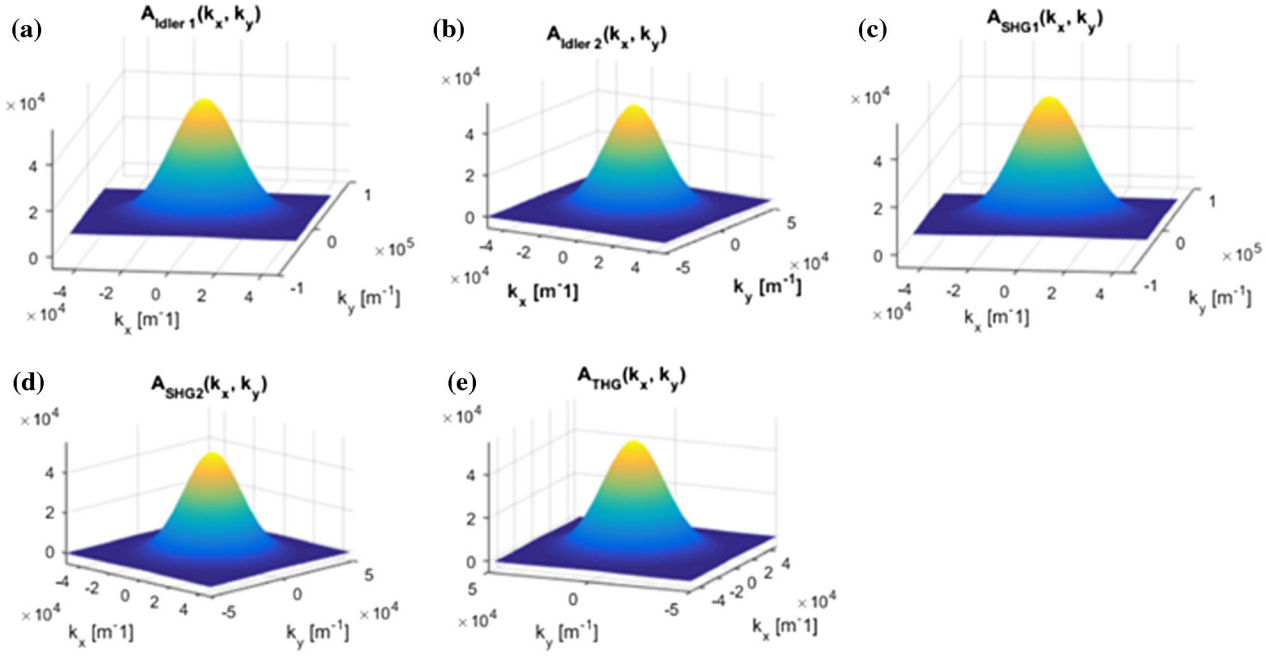

Fig. 5. Wavevector profiles for the simulated outputs at the (a) 600 nm, (b) 432 nm, (c) 490 nm, (d) 775 nm, and (e) 515 nm spectral regions.

biomedicine, high-density optical data storage, visible laser communications, laser-based color displays, and sensing.

Disclosures. The authors declare no conflicts of interest.

REFERENCES

1. Z. N. Zhang, Y. Bai, G. Z. Lei, B. Bai, Y. X. Sun, M. X. Hu, C. Wang, and J. T. Bai, "Wavelength tunable CW red laser generated based on an intracavity-SFG composite cavity," Laser Phys. Lett. **13**, 125402 (2016).
2. J. Sun, Y. Gan, and C. Xu, "Efficient green-light generation by proton-exchanged periodically poled MgO:$LiNbO_3$ ridge waveguide," Opt. Lett. **36**, 549–551 (2011).
3. R. Ji, S. Wang, Q. Liu, and W. Lu, "High-speed visible light communications: enabling technologies and state of the art," Appl. Sci. **8**, 589 (2018).
4. G. Ma, J. Yang, H. Tan, Y. Tian, W. Yao, Q. Ju, L. Zhang, J. Chen, X. Wu, and J. Gao, "Continuous-wave yellow laser generation at 578 nm by intracavity sum-frequency mixing of thin disk Yb:YAG laser and Nd:YAG laser," Opt. Laser Technol. **92**, 32–35 (2017).
5. K. Mizuuchi, K. Yamamoto, and M. Kato, "Harmonic blue light generation in X-cut MgO:$LiNbO_3$ waveguide," Electron. Lett. **33**, 806–807 (1997).
6. F. Brunner, E. Innerhofer, S. V. Marchese, T. Südmeyer, R. Paschotta, T. Usami, H. Ito, S. Kurimura, K. Kitamura, G. Arisholm, and U. Keller, "Powerful red–green–blue laser source pumped with a mode-locked thin disk laser," Opt. Lett. **29**, 1921–1923 (2004).
7. J. Capmany, "Simultaneous generation of red, green, and blue continuous-wave laser radiation in Nd^{3+}-doped aperiodically poled lithium niobate," Appl. Phys. Lett. **78**, 144–146 (2001).
8. J. Capmany, V. Bermúdez, D. Callejo, J. García Solé, and E. Diéguez, "Continuous wave simultaneous multi-self-frequency conversion in Nd^{3+}-doped aperiodically poled bulk lithium niobate," Appl. Phys. Lett. **76**, 1225–1227 (2000).
9. J. Liao, J. L. He, H. Liu, J. Du, F. Xu, H. T. Wang, S. N. Zhu, Y. Y. Zhu, and N. B. Ming, "Red, yellow, green and blue—four-color light from a single, aperiodically poled $LiTaO_3$ crystal," Appl. Phys. B **78**, 265–267 (2004).
10. J. Liao, J. L. He, H. Liu, H. T. Wang, S. N. Zhu, Y. Y. Zhu, and N. B. Ming, "Simultaneous generation of red, green, and blue quasi-continuous-wave coherent radiation based on multiple quasi-phase-matched interactions from a single, aperiodically-poled $LiTaO_3$," Appl. Phys. Lett. **82**, 3159–3161 (2003).
11. H. Lim, O. Prakash, B. Kim, K. Pandiyan, and M. Cha, "Ultra-broadband optical parametric generation in periodically poled lithium niobate and stoichiometric lithium tantalate crystals," Opt. Express **15**, 18294–18299 (2007).
12. Z. D. Gao, S. N. Zhu, S. Y. Tu, and A. H. Kung, "Monolithic red–green–blue laser light source based on cascaded wavelength conversion in periodically poled stoichiometric lithium tantalate," Appl. Phys. Lett. **89**, 181101 (2006).
13. P. Xu, L. N. Zhao, X. J. Lv, J. Lu, Y. Yuan, G. Zhao, and S. N. Zhu, "Compact high-power red–green–blue laser light source generation from a single lithium tantalate with cascaded domain modulation," Opt. Express **17**, 9509–9514 (2009).
14. D. K. Choge, H. Chen, Y. Xu, L. Guo, G. Li, and W. Liang, "Blue and orange two-color cw laser based on single-pass second-harmonic and sum-frequency generation in MgO:PPLN," Appl. Sci. **8**, 629 (2018).
15. B. E. A. Saleh and M. C. Teich, *Fundamentals of Photonics*, 2nd ed. (Wiley, 2007).
16. K. L. Baker, "Single-pass gain in a chirped quasi-phase-matched optical parametric oscillator," Appl. Phys. Lett. **82**, 3841–3843 (2003).
17. O. Gayer, Z. Sacks, E. Galun, and A. Arie, "Temperature and wavelength dependent refractive index equations for MgO-doped congruent and stoichiometric $LiNbO_3$," Appl. Phys. B **91**, 343–348 (2008).
18. A. Smith, "SNLO version 6.7 nonlinear optics software," http://www.as-photonics.com/snlo.
19. T. M. Kardaś, M. Nejbauer, P. Wnuk, B. Resan, C. Radzewicz, and P. Wasylczyk, "Full 3D modelling of pulse propagation enables efficient nonlinear frequency conversion with low energy laser pulses in a single-element tripler," Sci. Rep. **7**, 42889 (2017).